Cellular Physiology and Biochemistry

Cell Physiol Biochem 2018;51:1340-1353
DOI: 10.1159/000495552
Published online: 27 November 2018
Accepted: 19 November 2018

Original Paper

Ginsenoside 20(S)-Rg3 Prevents PKM2-Targeting miR-324-5p from H19 Sponging to Antagonize the Warburg Effect in Ovarian Cancer Cells

Xia Zheng[a,b] Yuanyuan Zhou[a,b] Wei Chen[c] Lihong Chen[d] Jiaojiao Lu[a,b] Fang He[a,b] Xu Li[a,b] Le Zhao[a,b]

[a]Center for Translational Medicine, the First Affiliated Hospital of Xi'an Jiaotong University, Xi'an, [b]Key Laboratory for Tumor Precision Medicine of Shaanxi Province, the First Affiliated Hospital of Xi'an Jiaotong University, Xi'an, [c]Center for Laboratory Medicine, the First Affiliated Hospital of Xi'an Jiaotong University, Xi'an, [d]Department of Obstetrics and Gynecology, Shaanxi Provincial People's Hospital, Xi'an, China

Key Words
Ginsenoside • Ovarian cancer • Warburg effect • Long non-coding RNA

Abstract
Background/Aims: The Warburg effect is one of the main metabolic features for cancers, with long non-coding RNA (lncRNA) being involved as a class of crucial regulators. Our previous studies have shown that ginsenoside 20(S)-Rg3, an active saponin monomer extracted from red ginseng, inhibits the Warburg effect in ovarian cancer cells. However, the detailed lncRNA regulatory network modulated by 20(S)-Rg3 to prevent the Warburg effect in ovarian cancer cells has not been explored. ***Methods:*** High-throughput sequencing was used to screen out the differentially expressed lncRNAs between 20(S)-Rg3-treated and non-treated SKOV3 cells. The levels of lncRNA H19 and miR-324-5p were manipulated in SKOV3 and A2780, and the glucose consumption, lactate production and PKM2 protein level were detected. Dual-luciferase reporter assay and RIP were utilized to verify the direct binding of H19 to miR-324-5p and miR-324-5p to PKM2. Cell proliferation was examined by CCK8 and colony formation assay. Nude mice subcutaneous xenograft tumor models were established to evaluate the impact of miR-324-5p on tumor growth *in vivo*. ***Results:*** 20(S)-Rg3 downregulated 67 lncRNAs, and H19 was one of the most decreased lncRNAs. Suppression of H19 by siRNA transfection reduced glucose consumption, lactate production and PKM2 expression in ovarian cancer cells, while H19 overexpression in 20(S)-Rg3-treated ovarian cancer cells enhanced glucose consumption, lactate production and PKM2 expression. Dual-luciferase reporter assay and RIP results showed that H19 directly bound to miR-324-5p. Dual-luciferase reporter assay showed that miR-324-5p directly targeted PKM2, and miR-324-5p negatively

X. Zheng and Y. Zhou contributed equally to this work.

Le Zhao, Ph.D
and Xu Li, Ph.D

Center for Translational Medicine, Key Laboratory for Tumor Precision Medicine of Shaanxi Province, the First Affiliated Hospital of Xi'an Jiaotong University, Xi'an, 710061 (China)
Tel. +86-29-85323528, E-Mail zhaole2@mail.xjtu.edu.cn; lixu56@mail.xjtu.edu.cn

regulated glucose consumption and lactate production in ovarian cancer cells. miR-324-5p overexpression inhibited cell proliferation *in vitro* and *in vivo*. ***Conclusion:*** Our study revealed that 20(S)-Rg3 blocked the competitive inhibition of H19 on miR-324-5p, which enhanced the suppression of miR-324-5p on PKM2 and therefore inhibited the Warburg effect and repressed tumorigenesis. In a word, 20(S)-Rg3 inhibited the Warburg effect in ovarian cancer cells via H19/miR-324-5p/PKM2 pathway.

Introduction

Ovarian cancer is the most lethal gynecological tumor, existing predominantly in the form of epithelial ovarian cancer (EOC). The estimated new cases of ovarian cancer are 22, 240, and the estimated deaths are 14, 070, which is 5% of deaths of females in the United States [1]. The 5-year survival has long been less than 50% in most countries [2]. Chemotherapy is the main adjuvant therapy for EOC, however, its efficacy is frequently impaired by occurrence of chemoresistance and adverse reaction [3]. Development of novel therapeutics is an important strategy to improve the prognosis of EOC patients.

Ginsenoside 20(S)-Rg3 is an active saponin monomer extracted from red ginseng, exerting anti-tumor function in multiple cancers [4]. A series of study have shown that 20(S)-Rg3 significantly inhibits ovarian cancer cells growth and metastasis partly via antagonizing the Warburg effect [5, 6]. The Warburg effect, also termed as aerobic glycolysis, is the main metabolic feature of cancers sustaining cancer cell growth under sufficient oxygen via rapidly generating ATP and biomaterials [7]. The Warburg effect is controlled by key glycolytic enzymes including hexokinase (HK), phosphofructokinase (PFK), pyruvate kinase (PK), and lactate dehydrogenase (LDH) [8]. Lately, long non-coding RNAs have been identified as a class of crucial regulators of the Warburg effect [9, 10]. However, the detailed lncRNA regulatory network modulated by 20(S)-Rg3 to prevent the Warburg effect in ovarian cancer cells has not been fully explored.

LncRNAs are a class of non-coding RNAs that are longer than 200 nucleotides implicated in tumor development and progression via regulating multiple genes expression to participate in various biological processes including metabolism, proliferation, apoptosis, migration and invasion. LncRNAs play their regulation role partly through acting as microRNA sponges to antagonize the binding of microRNA to their targets at 3' untranslated regions (3'UTRs) and therefore prevent microRNA-rendered promotion of RNA degradation or inhibition of translation. Increasing evidences have shown that lncRNAs regulate the Warburg effect in various cancers via sponging microRNAs [11, 12].

Here, we screen the differentially expressed lncRNAs between 20(S)-Rg3-treated and non-treated ovarian cancer cells via deep sequencing, and establish one lncRNA regulatory pathway modulated by 20(S)-Rg3 to prevent the Warburg effect in ovarian cancer cells. The results provide essential information for clinical translation of 20(S)-Rg3 for ovarian cancer therapy.

Materials and Methods

Drugs and antibodies

Ginsenoside 20(S)-Rg3 was obtained from Tasly Pharmaceutical Company (Tianjin, China). 20(S)-Rg3 was dissolved in DMSO, and then diluted in RPMI 1640 media at the concentration of 2 mg/ml as a stock solution and stored at -20℃ for later use. The primary antibodies against PKM2 (#4053) and β-actin (#3700) were from Cell Signaling Technology (Beverly, MA, USA), and the primary antibody against Ago2 (03-110) was from Millipore (Billerica, MA, USA).

Cell culture and treatment

The human ovarian cancer cell line SKOV3 was obtained from the Shanghai Cell Bank of Chinese Academy of Sciences (Shanghai, China), and A2780 was from the Shandong Academy of Medical Sciences (Jinan, China). Cells were cultured in RPMI 1640 with 10% fetal bovine serum (GIBCO; Grand Island, NY, USA) at 37°C, 5%CO_2 and incubated with 80 μg/mL (for SKOV3 cells) or 40 μg/mL (for A2780 cells) of 20(S)-Rg3 for 24 h or 48 h.

lncRNA deep sequencing and bioinformatics analysis

Deep sequencing was performed, and the data were analyzed by Novel Bioinformatics Ltd. Co. (Shanghai, China). Total RNAs were extracted from SKOV3 cells treated with 0 or 80 μg/mL 20(S)-Rg3 for 24 h by TRIzol reagent (Invitrogen; Carlsbad, CA, USA), and RNA with RIN>8.0 was utilized to construct rRNA depletion library (VAHTSTM Total RNA-seq (H/M/R)) according to the manufacturer's instructions. Raw data sequenced on the Ion Torrent Proton platform was filtered (removing the adaptor sequences, reads with >5% ambiguous bases (noted as N) and low-quality reads containing more than 20 percent of bases with qualities of <20). Clean data was then mapped to Human genome (GRCh38) utilizing HISAT2 algorithm [13]. HTSeq [14] was used to calculate the gene counts of lncRNAs. Differentially expressed lncRNA analysis was performed with DESeq algorithm [15] under following criteria: Fold Change>2, p-value<0.05 and FDR<0.05. The Miranda package [16] was used to predict microRNA target on the full length sequence of differentially expressed lncRNA.

Quantitative real-time PCR

Total RNA was extracted using TRIzol (Invitrogen; Carlsbad, CA, USA) and the concentrations were quantified on a UV spectrophotometer (Bio-Rad Inc.; Hercules, CA, USA). cDNA was synthesized according to the manufacturer's instructions of PrimeScript™ RT reagent kit with gDNA Eraser (TaKaRa; Dalian, China). Quantitative real-time PCR was performed on a CFX 96 real-time PCR system (Bio-Rad Inc,; Hercules, CA, USA) with SYBR Premix Ex Taq™ II kit (TaKaRa; Dalian, China). β-actin was used as internal control of lncRNA and mRNA, and U6 was the internal control of microRNA. Relative gene expression was calculated according to $2^{-\Delta\Delta Ct}$ method. The oligonucleotide primers were synthesized by BGI (Shenzhen, China) and microRNA primers were synthesized by RiboBio Co. Ltd. (Guangzhou, China). Sequences of primers were as follows:
H19 F 5'-TGC TGC ACT TTA CAA CCA CTG-3', R 5'-ATG GTG TCT TTG ATG TTG GGC-3';
PKM2 F 5'-TCC GGA TCT CTT CGT CTT TG-3', R 5'-GTC TGA ATG AAG GCA GTC CC-3';
β-actin F 5'-TCC CTG GAG AAG AGC TAC GA-3', R 5'-AGC ACT GTG TTG GCG TAC AG-3'.

Western blotting

Total protein was extracted using RIPA buffer containing protease inhibitors (Roche; Indianapolis, IN, USA). Protein concentrations were quantified with the BCA-200 Protein Assay kit (Pierce; Rockford, IL, USA). Proteins were separated on 10% SDS-polyacrylamide gels and transferred onto nitrocellulose membranes (Pall Life Science; Port Washington, NY, USA). Then the membranes were blocked in 5% non-fat milk at room temperature for 1 hour and incubated at 4°C overnight with the primary antibodies (PKM2 1:10000, β-actin 1:1000, Ago2 1:500). After washing with 0.5% TBST, the membranes were incubated with HRP-conjugated secondary antibodies, and the blots were developed using ECL reagents (Millipore; Billerica, MA, USA) by a chemiluminescence imaging system (Bio-Rad Inc., Hercules, CA, USA).

Glucose consumption and lactate production assay

The supernatant of cell culture media was collected to detect the levels of glucose and lactate separately with Glucose Assay kit and Lactic Acid Assay kit (Nanjing Jiancheng Bioengineering Institute; Nanjing, China) according to the manufacturer's instructions. The optical density at 505 nm for glucose measurement and 530 nm for lactate measurement were read on an EnSpire multimode plate reader (PerkinElmer; Waltham, MA, USA). Glucose consumption and lactate production were calculated based on the absorption values and normalized to the cell numbers.

miRNA inhibitor, miRNA mimic, small interfering RNA and plasmid transient transfection

hsa-miR-324-5p inhibitor and mimic were purchased from RiboBio Co. Ltd. (Guangzhou, China). H19 siRNAs were synthesized by GenePharma (Shanghai, China). Sequences of siRNAs were as follows: siH19-a5'-UAA GUC AUU UGC ACU GGU UTT-3'; siH19-b 5'-CCA ACA UCA AAG ACA CCA UTT-3'; negative control siRNA 5'-GCG ACG AUC UGC CUA AGA UTT-3'. The human H19-expressing plasmid was constructed by Genechem (Shanghai, China). Cells were seeded into 6-well plates. hsa-miR-324-5p inhibitor and mimic and H19 siRNAs were transfected at 30-50% confluency with X-treme GENE siRNA transfection reagent (Roche; Indianapolis, IN, USA) according to the manufacturer's instructions. The H19-expressing plasmid was transfected at 70-90% confluency with X-treme GENE HP DNA transfection reagent (Roche; Indianapolis, IN, USA). After 48 h or 72 h incubation, cells were harvested for further study.

Plasmid construction and dual-luciferase reporter assay

The human H19 gene and the 3'UTR of human PKM2 gene containing predicted miR-324-5p binding sites were amplified from genomic DNA of SKOV3 using the following primers:
H19 F 5'-CCC AAG CTT GGG CAG CCA CCA CAT CAT CCC AG-3', R 5'-GGA CTA GTC CCA GAG TCG TGG AGG CTT TGA-3';
PKM2 3'UTR F 5'-CCC AAG CTT GGG GGA GGA ATG CTG GAC TGG AG-3', R 5'-CCC AAG CTT GGG GGA GGA ATG CTG GAC TGG AG-3'.
The PCR products were recovered from running gels, digested with *Hind* III and *Spe* I endonuclease and inserted into pMIR-REPORT luciferase vector (Ambion; Austin, TX, USA) to construct H19-WT vector and PKM2-WT 3'UTR vector. The transversion mutants in the miR-324-5p binding sites were generated by overlap extension method to construct H19-MUT vector and PKM2-MUT 3'UTR vector. The primers were used as follows:
H19-MUT P1: 5'-CCCAAGCTTGGGCAGCCACCACATCATCCCAG-3',
P2: 5'-AGCTCCTCCAGCCTTCATACGCCGTCCCCACCA-3',
P3: 5'-TGGTGGGGACGGCGTATGAAGGCTGGAGGAGCT-3',
P4: 5'-GGACTAGTCCCAGAGTCGTGGAGGCTTTGA-3';
PKM2-MUT 3'UTR P1: 5'-CCCAAGCTTGGGGGAGGAATGCTGGACTGGAG-3',
P2: 5'-CCTTTAGAAAAAATCCTACGCCAGAGGACTCCC-3',
P3: 5'-GGGAGTCCTCTGGCGTAGGATTTTTTCTAAAGG-3',
P4: 5'-GGACTAGTCCTGGCTGTTTCTTGACCCCAA-3'.
All the recombinant vectors were confirmed by sequencing. Cells were seeded into 24-well plates. pRL-TK vectors (20 ng) and wild-type or mutation vectors (180 ng) were co-transfected along with 20 nM of miR-324-5p mimic or negative control at 80-90% confluency with X-treme GENE siRNA transfection reagent (Roche; Indianapolis, IN, USA) according to the manufacturer's instructions. 24 h after transfection, cells were harvested and the relative firefly luciferase activity (normalized to Renilla luciferase activity) was measured with Dual-Luciferase Reporter Assay System (Promega; Madison, WI, USA) according to the manufacturer's instructions.

RNA-binding protein immunoprecipitation

Cells were scraped off culture dishes and lysed using complete RIP lysis buffer at 80-90% confluency using Magna RIP kit (Millipore; Billerica, MA, USA). 100 µl of cell lysate was incubated with RIP immunoprecipitation buffer containing magnetic beads conjugated with anti-Ago2 antibody or normal mouse IgG at 4°C overnight. The immunoprecipitated RNA was purified by digesting protein with proteinase K and analyzed by qRT-PCR.

Lentivirus infection

hsa-miR-324-5p-up lentivirus was constructed by Genechem (Shanghai, China). The lentivirus infected cells with MOI 10 at 20-30% confluency. The cells were then used for cell viability assay, colony formation assay and xenograft tumor model.

Cell viability assay

1200 cells/well were seeded into 96-well plates. Cell viability was examined with Cell Counting Kit-8 (7seapharmtech Co. Ltd.; Shanghai, China) for 7 days. 10 μl of CCK-8 was added into 100 μl of culture media, and cells were incubated at 37°C for 0.5 h. The 450 nm wave-length absorption values were measured on an EnSpire multimode plate reader (PerkinElmer; Waltham, MA, USA). The detections were performed in triplicate wells on the same plate in three independent experiments.

Colony formation assay

500 cells/well were seeded into 6-well plates and cultured for 10 days. Cells were fixed with methanol and stained with crystal violet. The images were captured and the numbers of colonies in which the number of cells was more than 50 were counted under microscope.

Xenograft tumor model

All animal experimental procedures were approved by the Ethics Committee of the First Affiliated Hospital, Xi'an Jiaotong University. Four-week old BALB/c female mice were randomly divided into 2 groups (miR-324-5p and negative control, n=7) and injected subcutaneously with 2×10^6 cells (100 μl) into the right axilla. Mice weight and the length (L) and width (W) of xenograft tumors were measured every 3 days. Xenograft volume (V) was calculated as $V = (L \times W^2)/2$. The tumors were collected, weighed, and preserved in liquid nitrogen or formalin for further study at day 24.

Immunohistochemistry staining

Histologic slides were prepared from the paraffin-embedded subcutaneous xenograft tumor tissue blocks, and then dewaxed in xylene and rehydrated in a descending alcohol series. The specimens were heated in 0.01 M citrate buffer (pH 6.0) at 98°C for 20 minutes in a microwave oven to retrieve antigenic binding sites and incubated with anti-PKM2 antibody (1:800) at 4°C overnight. After incubation with HRP-conjugated secondary antibody at room temperature for 15 minutes, color was developed with DAB. Slides were counterstained with hematoxylin, dehydrated in an ascending alcohol series and mounted for analysis. Images were captured with an Olympus BH-2 microscope (Tokyo, Japan) installed with the DeltaPix Camera and software (Maalov, Denmark).

Statistical analysis

All data were represented as mean ± standard deviation and analyzed with SPSS software (Chicago, IL, USA). Statistical differences were determined by two-tailed t-test and considered significant (*) when $P<0.05$.

Results

Differential expression of lncRNAs in the 20(S)-Rg3-treated SKOV3 cells

LncRNA deep sequencing was performed to examine the 20(S)-Rg3-regulated lncRNAs in SKOV3 ovarian cancer cells. The raw lncRNA sequencing data was submitted to Gene Expression Omnibus (GEO) database and accessed with the GEO accession number GSE118216 (https://www.ncbi.nlm.nih.gov/geo/query/acc.cgi?acc=GSE118216). A total of 5305 lncRNAs were detected in 20(S)-Rg3-treated SKOV3 cells and negative control cells, including 1524 ncRNAs and 3781 pseudo genes. Compared to the control cells, 67 lncRNAs were significantly decreased (fold change<0.5, $p<0.05$) including 12 ncRNAs and 55 pseudo genes, and 18 lncRNAs were significantly increased (fold change>1.5, $p<0.05$) including 3 ncRNAs, 14 pseudo genes and 1 unknown gene in the 20(S)-Rg3-treated SKOV3 cells (Fig. 1A). The fold change (FC) and the corresponding false discovery rate (FDR) for the differentially expressed lncRNAs between 20(S)-Rg3-treated and non-treated SKOV3 cells were summarized in Table 1. Among the significantly differentially expressed lncRNAs, 4 lncRNAs presented the lowest FDR value (FDR=0) including downregulated pseudo gene RNU1-19P and ncRNA H19, and pseudo genes LOC93622 and CICP7.

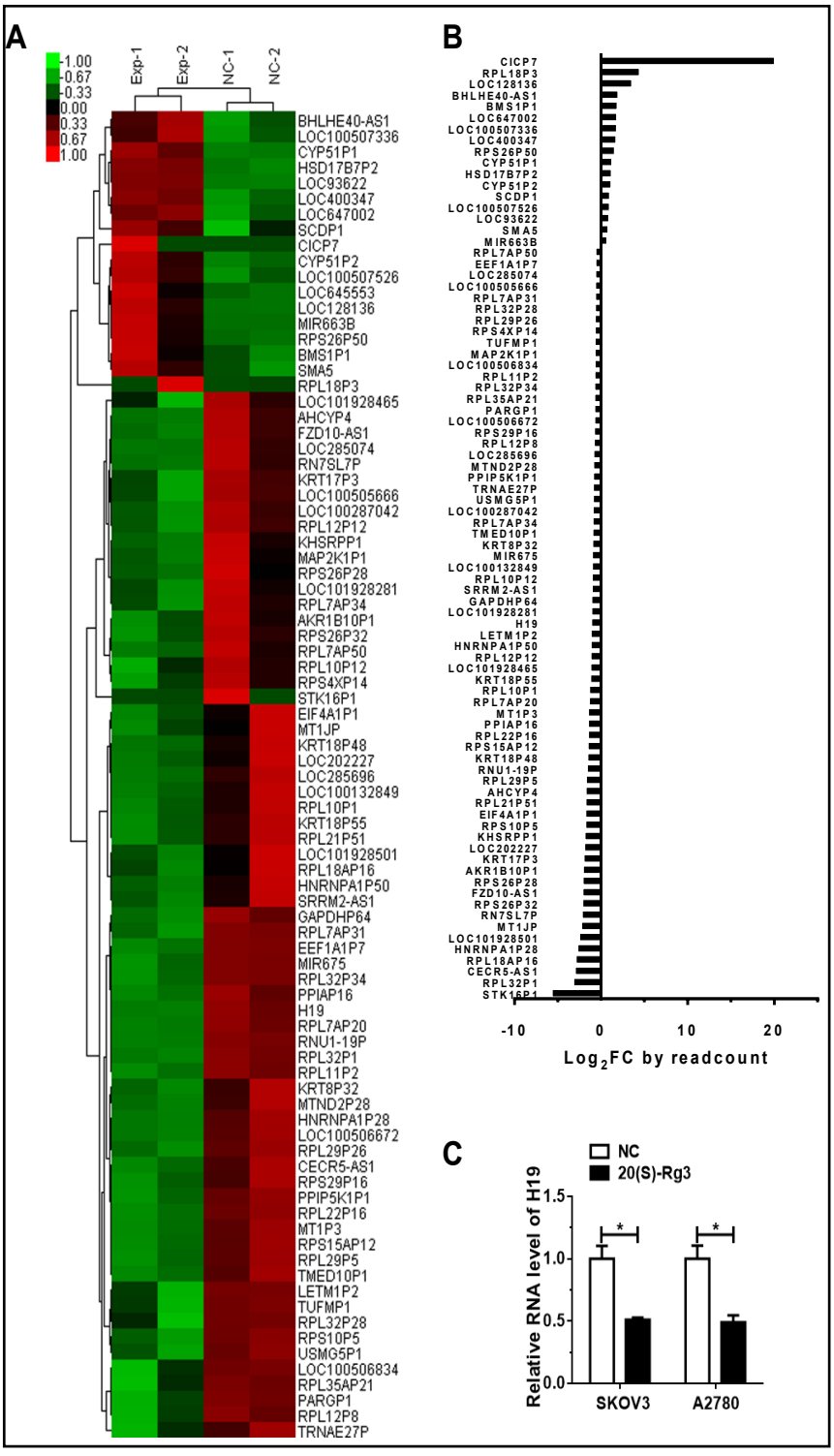

Fig. 1. The expression patterns of 85 differentially expressed lncRNAs in RNA-seq. (A) Hierarchical clustering of 85 differentially expressed lncRNAs in the 20(S)-Rg3-treated SKOV3 cells versus negative control cells were displayed in a heatmap (fold change of >1.5 or <0.5, FDR <0.05). Each column represented one library, and the color bar indicated the relative expression level from low (green) to high (red). EXP=20(S)-Rg3-treated SKOV3 cells. NC= negative control SKOV3 cells. (B) The expression $\log_2$FC (fold change, FC) values in the 20(S)-Rg3-treated SKOV3 cells versus negative control cells detected by RNA-seq were calculated by readcount. (C) Relative expression of the H19 was quantified by qRT-PCR. Compared with the control group, H19 was significantly decreased in the 20(S)-Rg3-treated group. *P<0.05, t-test.

20(S)-Rg3 downregulated H19 to inhibit the Warburg effect in ovarian cancer cells

H19 level was examined in 20(S)-Rg3-treated SKOV3 and A2780 ovarian cancer cells by qRT-PCR. Consistent with lncRNA deep sequencing results (Fig. 1B), H19 was found to be decreased by 50% in 20(S)-Rg3-treated cells compared to control cells (Fig. 1C). The role of H19 in the inhibition of 20(S)-Rg3 on the Warburg effect was then examined. Knocking down of H19 by siRNAs in SKOV3 and A2780 cells (Fig. 2A) reduced the glucose consumption

(Fig. 2B) and lactate production (Fig. 2C), and decreased PKM2 rather than HK2 expression (Fig. 2D). Overexpression of H19 in 20(S)-Rg3-treated SKOV3 and A2780 cells (Fig. 2E) reversed the inhibitory effect of 20(S)-Rg3 on the glucose consumption (Fig. 2F), lactate production (Fig. 2G) and PKM2 expression (Fig. 2H), but had no effect on HK2 expression. These results indicated that 20(S)-Rg3 prevented the Warburg effect via suppressing H19 expression in ovarian cancer cells.

Table 1. The top thirty lncRNAs most significantly changed in 20(S)-Rg3-treated SKOV3 cells relative to negative control cells

Accession ID	20(S)-Rg3	NC	Fold change	FDR
RNU1-19P	116.652054	347.1274	0.336049689	0
H19	4660.3653	9894.069	0.471026155	0
RPL29P26	257.340143	408.841	0.629438135	4.01E-09
RPS15AP12	34.9791677	98.16263	0.356338937	7.64E-09
RPL7AP31	275.912635	426.1764	0.64741414	3.06E-08
RPL12P12	63.5927035	141.7483	0.448631103	1.23E-07
RPL32P1	3.74074726	33.38363	0.112053351	1.61E-07
RPL32P34	174.994415	287.0565	0.609616596	2.83E-07
RN7SL7P	164.338415	737.2274	0.222914142	5.11E-07
RPS10P5	19.2780015	65.55466	0.294075232	8.24E-07
LOC285074	165.23248	252.8701	0.653428211	1.89E-06
MTND2P28	191.442355	346.2095	0.552966815	5.12E-06
KRT17P3	11.5340185	45.02861	0.256148693	8.6E-06
TMED10P1	74.9788573	143.4249	0.522774159	1.28E-05
KRT8P32	66.1849204	129.1888	0.512311555	1.4E-05
RPL32P28	161.844774	252.5958	0.640726365	1.81E-05
PARGP1	111.975977	184.9885	0.605313134	1.91E-05
RPS26P32	23.5763935	102.3762	0.230291674	7.47E-05
LOC100506672	120.54869	199.6582	0.603775283	9.96E-05
RPL11P2	122.72253	200.1663	0.613102926	0.000175
GAPDHP64	45.8323209	96.0118	0.477361339	0.000327
RPL21P51	13.8144587	46.03459	0.300088696	0.000336
FZD10-AS1	7.48149453	31.97119	0.234007379	0.000621
PPIP5K1P1	67.4973628	122.7634	0.549816613	0.000652
LOC285696	62.2636407	109.9736	0.566169082	0.000719
AHCYP4	12.3214839	40.85565	0.301585783	0.000748
KRT18P55	36.4967867	83.38794	0.437674653	0.001374
PPIAP16	17.8423386	48.56139	0.367418201	0.001608
LOC100506834	145.125749	232.7742	0.623461356	0.001913
STK16P1	2.06723998	102.8301	0.020103451	0.00197

H19 sponged miR-324-5p to enhance PKM2 expression

We then investigated the mechanism of the stimulation of H19 on PKM2 expression. Since H19 was found to act as the microRNAs sponge, we attempted to identify a PKM2-targeting microRNA sponged by H19. We previously reported that 11 microRNAs were significantly upregulated by 20(S)-Rg3, including miR-3163, miR-664a-5p, miR-6717-5p, miR-4329, miR-603, miR-324-5p, miR-1283, miR-532-3p, miR-33a-3p, miR-519a-5p and miR-486-3p. Analysis using RNAHybrid algorithm found a binding site of miR-324-5p in H19 sequence located in 1897-1902nt, and PKM2 was predicted as a potential target of miR-324-5p by microRNA.org database. Knocking down of H19 increased miR-324-5p level (Fig. 3A), while overexpression of H19 abrogated the 20(S)-Rg3-stimulated miR-324-5p (Fig. 3B). But inhibition of miR-324-5p in 20(S)-Rg3-treated cells or overexpression of miR-324-5p did not influence the level of H19 (Fig. 3C and 3D). These results indicated H19 negatively regulated miR-324-5p, but not vice versa.

The direct action of H19 on miR-324-5p was further verified by dual-luciferase reporter assay and RNA-binding protein immunoprecipitation (RIP). Dual-luciferase reporter assay showed that miR-324-5p mimic weakened the luciferase activity of H19 WT luciferase reporter vector containing the wild-type miR-324-5p-binding site in H19 sequence, while it had no effect on that of H19 MUT luciferase reporter vector containing the mutant miR-324-5p-binding site (Fig. 3E). RIP for Ago2 followed by qRT-PCR showed that endogenous H19 and miR-324-5p were specifically enriched in the component pulled down by anti-Ago2 antibody (Fig. 3F), manifesting that H19 was associated with RNA-induced silencing complex composed of miR-324-5p and Ago2 protein.

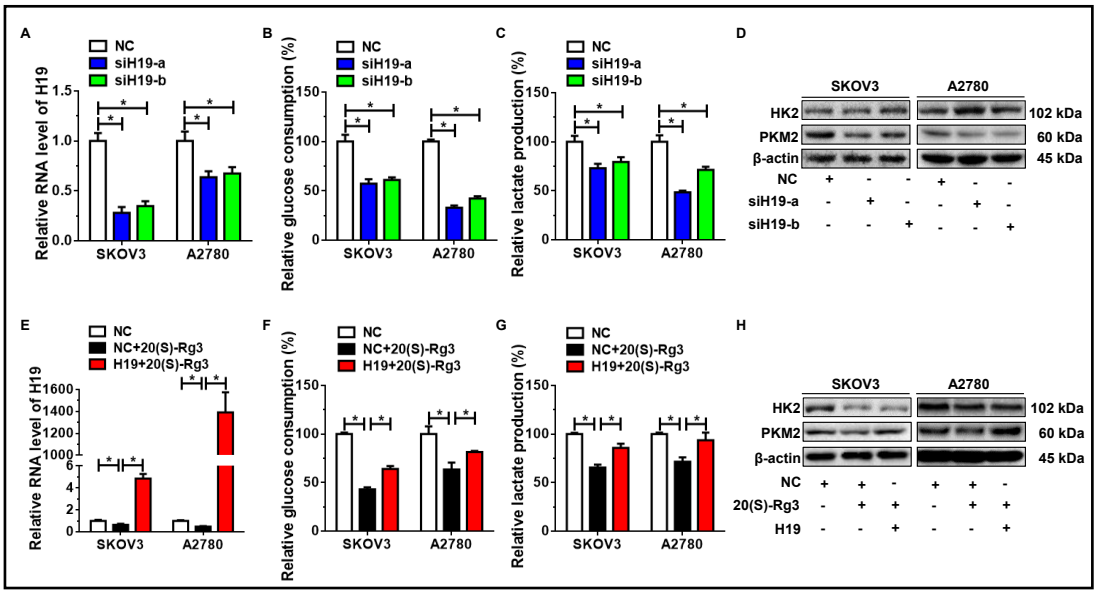

Fig. 2. 20(S)-Rg3 downregulated H19 to antagonize the Warburg effect. (A) H19 was effectively knocked down by two siRNA in both SKOV3 and A2780 ovarian cancer cells after 48 h transfection. (B) Knocking down of H19 inhibited glucose consumption of SKOV3 and A2780 cells. (C) Knocking down of H19 weakened lactate production in SKOV3 and A2780 cells. (D) Knocking down of H19 reduced PKM2 protein level, while had insignificant effect on HK expression level. (E) H19 was decreased in 20(S)-Rg3-treated cells, and H19 was overexpressed in 20(S)-Rg3-treated cells after transfection of H19-expressing plasmid for 48 h. (F) 20(S)-Rg3 lessened glucose consumption in SKOV3 and A2780 ovarian cancer cells, which was partly recovered by H19 overexpression. (G) H19 overexpression impaired the inhibition of 20(S)-Rg3 on lactate production. (H) H19 overexpression reversed the function of 20(S)-Rg3 on decreasing PKM2. *P<0.05, t-test.

Next we knocked down both of H19 and miR-324-5p in SKOV3 and A2780 (Fig. 3G). The reduction of glucose consumption and lactate production caused by H19 interference was prevented by miR-324-5p inhibition (Fig. 3H and 3I). Meanwhile, the protein level of PKM2 in H19 and miR-324-5p co-inhibited cells was increased compared with that in H19-inhibited cells (Fig. 3J). These results illustrated that H19 enhanced PKM2 expression to promote the Warburg effect in ovarian cancer cells by sponging miR-324-5p.

miR-324-5p antagonized the Warburg effect via directly inhibiting PKM2

The effect of miR-324-5p on the Warburg effect in ovarian cancer cells was then examined. Overexpression of miR-324-5p via transfecting miR-324-5p mimic into SKOV3 and A2780 cells (Fig. 4A) reduced the glucose consumption (Fig. 4B) and lactate production (Fig. 4C), and significantly decreased PKM2 protein level (Fig. 4D). Next miR-324-5p was suppressed via transfecting miR-324-5p inhibitor into 20(S)-Rg3-treated SKOV3 and A2780 cells. qRT-PCR results showed that miR-324-5p inhibitor antagonized 20(S)-Rg3-induced elevation of miR-324-5p (Fig. 4E), and reduction of glucose consumption (Fig. 4F), lactate production (Fig. 4G) and PKM2 protein level (Fig. 4H). These results indicated that 20(S)-Rg3 inhibited the Warburg effect in ovarian cancer cells by upregulating miR-324-5p.

Online algorithm (microRNA.org) predicted the miR-324-5p-binding site was located in 331-336nt of PKM2 3'UTR. We constructed PKM2 WT-3'UTR containing the miR-324-5p-binding site and PKM2 MUT-3'UTR containing transversion mutations of the miR-324-5p-binding site. Dual-luciferase reporter assay showed that compared with the negative control, miR-324-5p mimics significantly decreased the luciferase activity of PKM2 WT-3'UTR, but had no effect on the luciferase activity of PKM2 MUT-3'UTR (Fig. 4I). These data verified that miR-324-5p directly targeted PKM2.

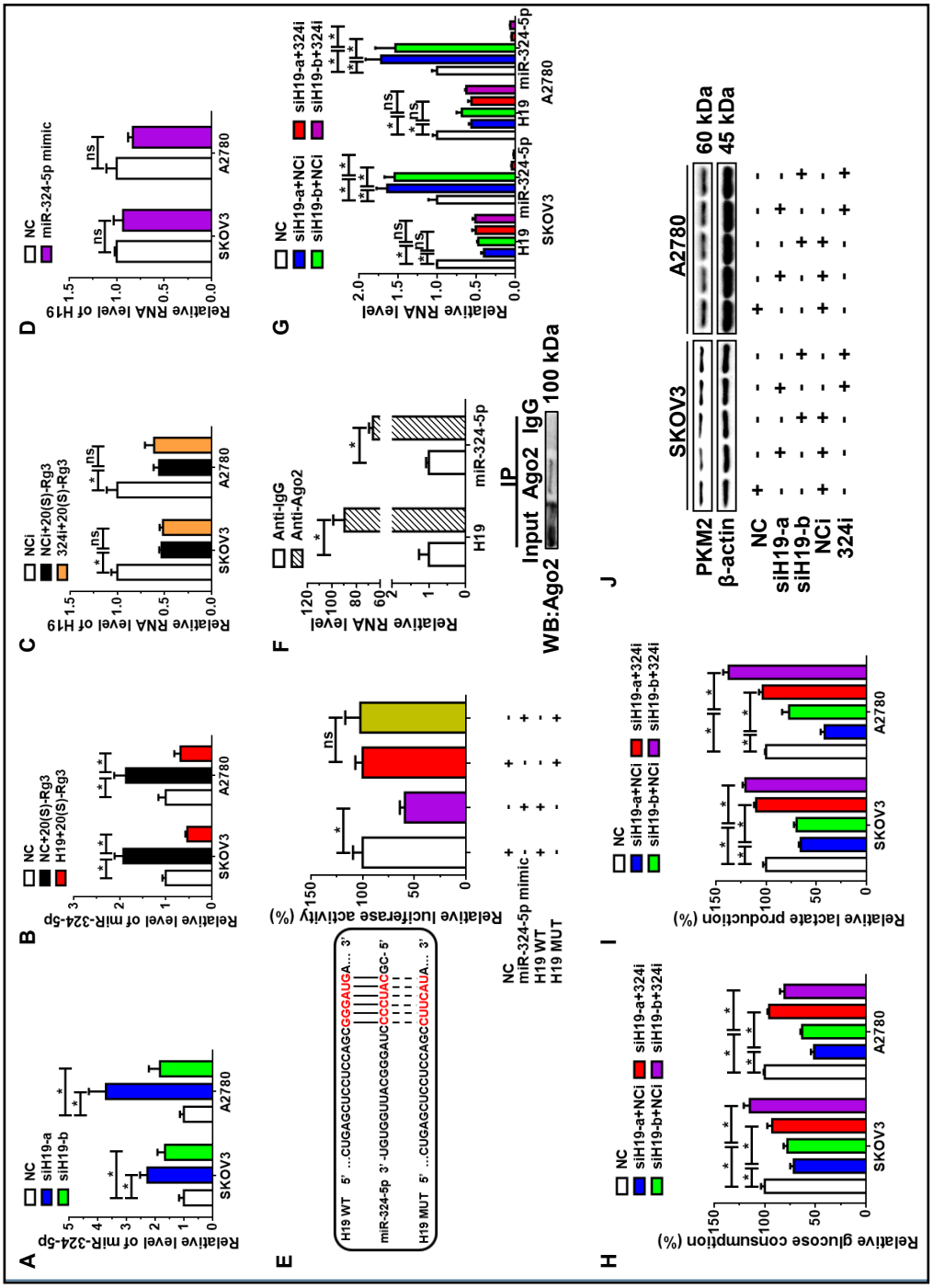

Fig. 3. H19 sponged miR-324-5p to promote the Warburg effect. (A) qRT-PCR results showed that knocking down of H19 increased miR-324-5p level. (B) H19 overexpression reversed the elevation of miR-324-5p by 20(S)-Rg3. (C) miR-324-5p suppression did not rescue H19 in 20(S)-Rg3-treated cells. (D) miR-324-5p overexpression had no effect on H19 level. (E) Dual luciferase reporter assay showed that miR-324-5p directly bound to H19. (F) RIP indicated that H19 bound to the RNA-induced silencing complex containing Ago2 protein. (G) miR-324-5p inhibition suppressed the siH19-induced miR-324-5p elevation. (H) miR-324-5p repression impaired the siH19-induced decrease of glucose consumption in ovarian cancer cells. (I) miR-324-5p repression impaired the siH19-induced decrease of lactate production in ovarian cancer cells. (J) miR-324-5p suppression reversed the function of siH19 on decreasing PKM2. *P<0.05, t-test.

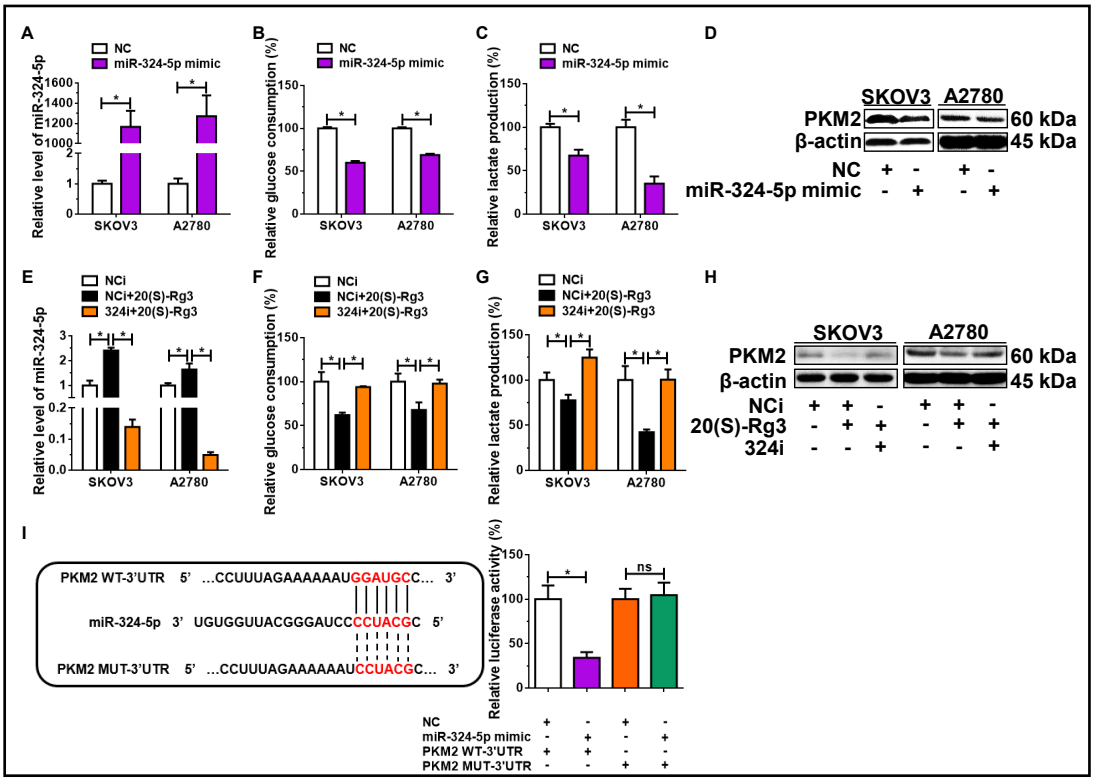

Fig. 4. miR-324-5p targeted PKM2 to antagonize the Warburg effect. (A) qRT-PCR showed that miR-324-5p was overexpressed by miR-324-5p mimic transfection. (B) Glucose consumption was reduced in miR-324-5p overexpressed cells. (C) Lactate production were reduced in miR-324-5p overexpressed cells. (D) PKM2 protein level was decreased in miR-324-5p mimic-transfected ovarian cancer cells. (E) qRT-PCR results showed that miR-324-5p was inhibited by miR-324-5p inhibitor transfection. (F) miR-324-5p suppression impaired the inhibition of 20(S)-Rg3 on the glucose consumption. (G) miR-324-5p suppression impaired the inhibition of 20(S)-Rg3 on the lactate production. (H) miR-324-5p suppression reversed the function of 20(S)-Rg3 on decreasing PKM2. (I) Dual-luciferase reporter assay showed that PKM2 was the direct target of miR-324-5p. *P<0.05, t-test.

Overexpression of miR-324-5p inhibited ovarian cancer cell proliferation in vitro and in vivo

To verify the influence of the anti-Warburg effect of miR-324-5p in ovarian cancer cells, SKOV3 cells were infected by hsa-miR-324-5p-up lentivirus to overexpress miR-324-5p (Fig. 5A), and cell proliferation was examined. Compared with the negative control, overexpression of miR-324-5p significantly retarded cell viability (Fig. 5B) and colony formation capability (Fig. 5C), illustrating that miR-324-5p inhibited ovarian cancer cell proliferation *in vitro*. We then checked the effect of miR-324-5p on the proliferation of ovarian cancer cells *in vivo*. Nude mice subcutaneous xenograft models were established using miR-324-5p-up SKOV3 cells and negative control cells, respectively. The mice body weights in negative control group and miR-324-5p-up group were comparable (Fig. 5D). But compared with the negative control group, the tumorigenicity of miR-324-5p-up cells was substantially impaired as illustrated by the fewer xenografts and smaller tumor volumes (Fig. 5E and 5F). qRT-PCR results of xenograft tissues showed that miR-324-5p was increased while H19 remained unchanged in miR-324-5p-up group relative to those of the negative control group (Fig. 5G). Immunohistochemistry results showed that PKM2 protein level was decreased in miR-324-5p-up group compared to that in negative control group (Fig. 5H).

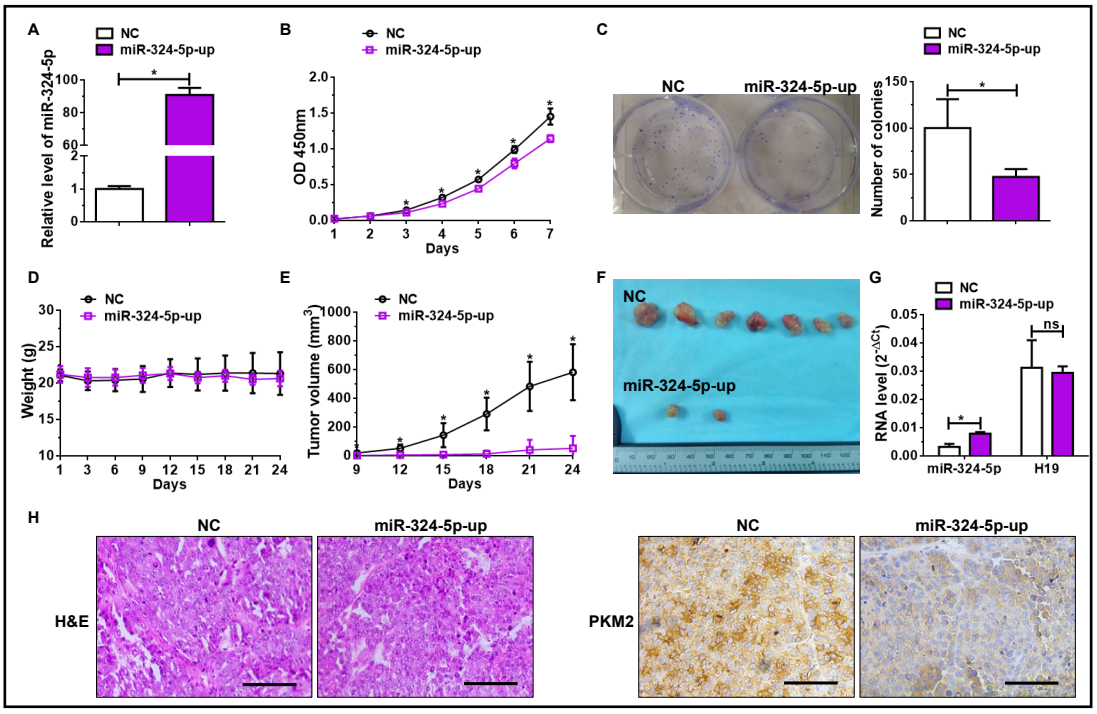

Fig. 5. Overexpression of miR-324-5p inhibited ovarian cancer tumorigenesis in vitro and vivo. (A) miR-324-5p was overexpressed in hsa-miR-324-5p-up lentivirus-infected SKOV3 cells. (B) Cell growth of miR-324-5p overexpressed cells was retarded relative to the negative control cells. (C) miR-324-5p overexpression inhibited cell capability of plate colony formation. (D) The mice weights of miR-324-5p-up and control groups were comparable. (E) Tumor volumes of subcutaneous xenografts in miR-324-5p-up group were substantially smaller than those of control group. (F) Compared to control group, tumor formation of subcutaneous xenograft in miR-324-5p-up group was significantly inhibited. (G) The level of miR-324-5p was increased, whereas the levels of H19 did not change in miR-324-5p-up group compared with the negative control. (H) Immunohistochemical staining of PKM2 in xenograft tumor tissues (bar scale 50μm) showed that PKM2 protein level was reduced in miR-324-5p-up group. *P<0.05, t-test.

Discussion

The Warburg effect is one of the main metabolism ways for ovarian cancer. Research and development of novel therapeutics targeting the Warburg effect will be a feasible strategy to enhance the efficacy of first-line chemotherapeutic drugs and reduce adverse reaction in EOC patients [17]. 20(S)-Rg3 exhibits anti-tumor activity in various cancers via inducing apoptosis or weakening proliferation, migration and invasion of cancer cells [18-20]. Our previous studies have found that 20(S)-Rg3 antagonized the Warburg effect in ovarian cancer and downregulates the two key glycolytic enzymes HK2 and PKM2 [5, 6]. Mechanistic studies have revealed that 20(S)-Rg3 downregulates HK2 via STAT3 [5] or DNMT3A/miR-532-3p [6] pathways. But the mechanism of PKM2 downregulation induced by 20(S)-Rg3 remains unknown.

We proceeded to investigate the PKM2 downregulation pathway based on previously acquired microRNA sequencing data [6]. PKM2 was predicted and experimentally confirmed as the direct target of 20(S)-Rg3-upregulated miR-324-5p. In view of accumulating evidence proving lncRNAs as microRNA sponges to negatively regulate microRNA function [21-23], we identified the 20(S)-Rg3-influenced lncRNA expression profile with deep sequencing technique to investigate the lncRNA competitively binding miR-324-5p. Fortunately, H19 was screened out from 67 20(S)-Rg3-reduced lncRNAs, with the binding site of miR-324-5p in its sequence. The competitive binding of H19 to miR-324-5p rescued PKM2 from being

translationally inhibited by miR-324-5p. H19/miR-324-5p/PKM2 pathway was therefore established as the anti-Warburg mechanism of 20(S)-Rg3.

H19 was overexpressed in various cancers including ovarian cancer, and capable of stimulating cancer cell cycle progression, proliferation, migration and invasion [24, 25]. H19 facilitated tumor development and progression partly via sponging microRNA to recover the expression of microRNA-targeted genes [26-28]. Recently H19 was found to promote glucose metabolism and cell growth in malignant melanoma via competitively binding miR-106a-5p to release E2F3 [29]. Here we identified PKM2-targeting miR-324-5p as another target microRNA sponged by H19, and H19 therefore was a pro-Warburg lncRNA while miR-324-5p was an anti-Warburg microRNA. miR-324-5p has been reported as both oncomiR and tumor repressor in cancers because it inhibited cell growth and invasion in multiple myeloma and hepatocellular cancer [30], while promoted proliferation, migration and invasion of papillary thyroid microcarcinoma cells and breast cancer cells [31, 32]. But most published results were from *in vitro* data. Here, miR-324-5p was verified *in vitro* and *in vivo* as a suppressor of ovarian cancer proliferation via negatively regulating the Warburg effect.

In this study, we first reported the 20(S)-Rg3-regulated lncRNA expression profile and identified H19/miR-324-5p/PKM2 pathway responsible for the anti-Warburg activity of 20(S)-Rg3. Further study of 20(S)-Rg3-regulated lncRNA and microRNA could contribute to the understanding of both anti-cancer action of 20(S)-Rg3 and progression mechanism of ovarian cancer.

Conclusion

Our results indicated that 20(S)-Rg3 inhibited the Warburg effect via H19/miR-324-5p/PKM2 pathway to retard growth of ovarian cancer cells.

Acknowledgements

This work was supported by the National Natural Science Foundation of China (No. 81702576 and No. 30973429), the Natural Science Foundation of Shaanxi Province (No. 2017JM8107) and Foundation of the First Affiliated Hospital of Xi'an Jiaotong University (No. 2016QN-10).

Disclosure Statement

The authors declare no conflicts of interest.

References

1 Siegel RL, Miller KD, Jemal A: Cancer statistics, 2018. CA Cancer J Clin 2018;68:7-30.
2 Allemani C, Matsuda T, Di Carlo V, Harewood R, Matz M, Niksic M, Bonaventure A, Valkov M, Johnson CJ, Esteve J, Ogunbiyi OJ, Azevedo ESG, Chen WQ, Eser S, Engholm G, Stiller CA, Monnereau A, Woods RR, Visser O, Lim GH et al.: Global surveillance of trends in cancer survival 2000-14 (CONCORD-3): analysis of individual records for 37 513 025 patients diagnosed with one of 18 cancers from 322 population-based registries in 71 countries. Lancet 2018;10.1016/S0140-6736(17)33326-3.
3 Kroeger PT, Jr., Drapkin R: Pathogenesis and heterogeneity of ovarian cancer. Curr Opin Obstet Gynecol 2017;29:26-34.
4 Nag SA, Qin JJ, Wang W, Wang MH, Wang H, Zhang R: Ginsenosides as Anticancer Agents: *In vitro* and *in vivo* Activities, Structure-Activity Relationships, and Molecular Mechanisms of Action. Front Pharmacol 2012;3:25.

5 Li J, Liu T, Zhao L, Chen W, Hou H, Ye Z, Li X: Ginsenoside 20(S)Rg3 inhibits the Warburg effect through STAT3 pathways in ovarian cancer cells. Int J Oncol 2015;46:775-781.
6 Zhou Y, Zheng X, Lu J, Chen W, Li X, Zhao L: Ginsenoside 20(S)-Rg3 Inhibits the Warburg Effect Via Modulating DNMT3A/ MiR-532-3p/HK2 Pathway in Ovarian Cancer Cells. Cell Physiol Biochem 2018;45:2548-2559.
7 Pavlova NN, Thompson CB: The Emerging Hallmarks of Cancer Metabolism. Cell Metab 2016;23:27-47.
8 Yu L, Chen X, Sun X, Wang L, Chen S: The Glycolytic Switch in Tumors: How Many Players Are Involved? J Cancer 2017;8:3430-3440.
9 Xiang S, Gu H, Jin L, Thorne RF, Zhang XD, Wu M: LncRNA IDH1-AS1 links the functions of c-Myc and HIF1alpha via IDH1 to regulate the Warburg effect. Proc Natl Acad Sci U S A 2018;115:E1465-E1474.
10 Li Z, Li X, Wu S, Xue M, Chen W: Long non-coding RNA UCA1 promotes glycolysis by upregulating hexokinase 2 through the mTOR-STAT3/microRNA143 pathway. Cancer Sci 2014;105:951-955.
11 Ye H, Zhou Q, Zheng S, Li G, Lin Q, Ye L, Wang Y, Wei L, Zhao X, Li W, Fu Z, Liu Y, Li Z, Chen R: FEZF1-AS1/ miR-107/ZNF312B axis facilitates progression and Warburg effect in pancreatic ductal adenocarcinoma. Cell Death Dis 2018;9:34.
12 Song J, Wu X, Liu F, Li M, Sun Y, Wang Y, Wang C, Zhu K, Jia X, Wang B, Ma X: Long non-coding RNA PVT1 promotes glycolysis and tumor progression by regulating miR-497/HK2 axis in osteosarcoma. Biochem Biophys Res Commun 2017;490:217-224.
13 Kim D, Langmead B, Salzberg SL: HISAT: a fast spliced aligner with low memory requirements. Nat Methods 2015;12:357-360.
14 Anders S, Pyl PT, Huber W: HTSeq--a Python framework to work with high-throughput sequencing data. Bioinformatics 2015;31:166-169.
15 Anders S, Huber W: Differential expression analysis for sequence count data. Genome Biol 2010;11:R106.
16 Enright AJ, John B, Gaul U, Tuschl T, Sander C, Marks DS: MicroRNA targets in Drosophila. Genome Biol 2003;5:R1.
17 Suh DH, Kim HS, Kim B, Song YS: Metabolic orchestration between cancer cells and tumor microenvironment as a co-evolutionary source of chemoresistance in ovarian cancer: a therapeutic implication. Biochem Pharmacol 2014;92:43-54.
18 Lee JY, Jung KH, Morgan MJ, Kang YR, Lee HS, Koo GB, Hong SS, Kwon SW, Kim YS: Sensitization of TRAIL-induced cell death by 20(S)-ginsenoside Rg3 via CHOP-mediated DR5 upregulation in human hepatocellular carcinoma cells. Mol Cancer Ther 2013;12:274-285.
19 Li J, Lu J, Ye Z, Han X, Zheng X, Hou H, Chen W, Li X, Zhao L: 20(S)-Rg3 blocked epithelial-mesenchymal transition through DNMT3A/miR-145/FSCN1 in ovarian cancer. Oncotarget 2017;8:53375-53386.
20 Yuan HD, Quan HY, Zhang Y, Kim SH, Chung SH: 20(S)-Ginsenoside Rg3-induced apoptosis in HT-29 colon cancer cells is associated with AMPK signaling pathway. Mol Med Rep 2010;3:825-831.
21 Salmena L, Poliseno L, Tay Y, Kats L, Pandolfi PP: A ceRNA hypothesis: the Rosetta Stone of a hidden RNA language? Cell 2011;146:353-358.
22 Tay Y, Rinn J, Pandolfi PP: The multilayered complexity of ceRNA crosstalk and competition. Nature 2014;505:344-352.
23 Thomson DW, Dinger ME: Endogenous microRNA sponges: evidence and controversy. Nat Rev Genet 2016;17:272-283.
24 Medrzycki M, Zhang Y, Zhang W, Cao K, Pan C, Lailler N, McDonald JF, Bouhassira EE, Fan Y: Histone h1.3 suppresses h19 noncoding RNA expression and cell growth of ovarian cancer cells. Cancer Res 2014;74:6463-6473.
25 Zhong Y, Gao D, He S, Shuai C, Peng S: Dysregulated Expression of Long Noncoding RNAs in Ovarian Cancer. Int J Gynecol Cancer 2016;26:1564-1570.
26 Lv M, Zhong Z, Huang M, Tian Q, Jiang R, Chen J: lncRNA H19 regulates epithelial-mesenchymal transition and metastasis of bladder cancer by miR-29b-3p as competing endogenous RNA. Biochim Biophys Acta 2017;1864:1887-1899.
27 Li Z, Li Y, Ren K, Li X, Han X, Wang J: Long non-coding RNA H19 promotes the proliferation and invasion of breast cancer through upregulating DNMT1 expression by sponging miR-152. J Biochem Mol Toxicol 2017;31. doi:10.1002/jbt.21933.

28 Zhou W, Ye XL, Xu J, Cao MG, Fang ZY, Li LY, Guan GH, Liu Q, Qian YH, Xie D: The lncRNA H19 mediates breast cancer cell plasticity during EMT and MET plasticity by differentially sponging miR-200b/c and let-7b. Sci Signal 2017;10:pii:eaak9557.

29 Luan W, Zhou Z, Ni X, Xia Y, Wang J, Yan Y, Xu B: Long non-coding RNA H19 promotes glucose metabolism and cell growth in malignant melanoma via miR-106a-5p/E2F3 axis. J Cancer Res Clin Oncol 2018;144:531-542.

30 Tang B, Xu A, Xu J, Huang H, Chen L, Su Y, Zhang L, Li J, Fan F, Deng J, Tang L, Sun C, Hu Y: MicroRNA-324-5p regulates stemness, pathogenesis and sensitivity to bortezomib in multiple myeloma cells by targeting hedgehog signaling. Int J Cancer 2018;142:109-120.

31 Yang Y, Xia S, Ni X, Ni Z, Zhang L, Wang W, Kong Y, Wang Y, Ye L, Zhan W: MiR-324-5p assists ultrasonography in predicting lymph node metastasis of unifocal papillary thyroid microcarcinoma without extracapsular spread. Oncotarget 2017;8:83802-83816.

32 Song L, Liu D, Zhao Y, He J, Kang H, Dai Z, Wang X, Zhang S, Zan Y: Sinomenine inhibits breast cancer cell invasion and migration by suppressing NF-kappaB activation mediated by IL-4/miR-324-5p/CUEDC2 axis. Biochem Biophys Res Commun 2015;464:705-710.